

## OBSERVATIONS OF C<sub>3</sub> IN COMET 9P/TEMPEL 1 DURING *DEEP IMPACT*

MÁTÉ ÁDÁMKOVICS, IMKE DE PATER, AND HYRON SPINRAD  
Astronomy Department, University of California, Berkeley, CA 94720  
*Draft version October 24, 2006*

### ABSTRACT

The 4050 Å band of C<sub>3</sub> has been observed with Keck/HIRES during the *Deep Impact* encounter. We measure the gradual increase and subsequent decline of the C<sub>3</sub> production rate during the 4 hours after impact. The quiescent production rate of C<sub>3</sub> before the encounter was  $1.0 \times 10^{23} \text{ s}^{-1}$ , while 2 hours after impact we recorded a peak production rate of  $1.7 \times 10^{23} \text{ s}^{-1}$ . The rotational population distribution was observed to change with time, beginning with a rotational excitation temperature of  $\sim 45 \text{ K}$  at impact and increasing for 2 hrs up to a maximum of  $61 \pm 5 \text{ K}$ . During the interval from 2 to 4 hr after impact the C<sub>3</sub> excitation temperature returned to the pre-impact value while the C<sub>3</sub> production rate remained elevated until the end of the observations. These observations are interpreted in terms of changing gas densities in the coma and short-term changes in the primary production mechanism for C<sub>3</sub>.

*Subject headings:* comets: general — comets: individual (9P/Tempel 1) — molecular processes

### 1. INTRODUCTION

The first compositional analyses from the *Deep Impact* (*DI*) mission are now emerging and suggest that there is not a dramatic difference between the chemical composition of the interior and surface layers of comet 9P/Tempel 1. Feldman et al. (2006) use ultraviolet observations to show that the amount of CO relative to H<sub>2</sub>O is similar in both the impact ejecta and in the outgassing of the quiescent comet. Jehin et al. (2006) measured <sup>12</sup>C/<sup>13</sup>C and <sup>14</sup>N/<sup>15</sup>N in the material released by impact and find it to be the same as the surface material. Mumma et al. (2005) show that the relative abundances of CH<sub>3</sub>OH and HCN are the same before and after impact, although the amount of C<sub>2</sub>H<sub>6</sub> relative to H<sub>2</sub>O increases by almost a factor of two shortly after impact. Schleicher et al. (2006) report that in nearly all respects — including the production rate of C<sub>3</sub> — comet 9P/Tempel 1 returned to pre-impact conditions within 6 days. With the precisely timed outburst caused by *DI*, the short (4 hr) time period directly after impact offers a unique opportunity to observe molecular formation mechanisms that occur on short timescales. Here we describe the observed variations in the excitation temperature and production rate of C<sub>3</sub> in the first four hours after *DI*.

### 2. OBSERVATIONS AND REDUCTION

The observations were conducted using the HIRES cross-dispersed echelle spectrometer (Vogt et al. 1994) at the W.M. Keck observatory and made publicly available via the Keck Observatory Archive (KOA) (Cochran et al. 2006). Preliminary analysis and description of the observations is also given in Jehin et al. (2006). Briefly, HIRES offers nearly complete spectral coverage from 3000 – 5880 Å at a spectral resolution,  $\lambda/\Delta\lambda \sim 48,000$  with a 0.85" slit and a 0.239" plate scale. Three 20 min exposures were taken on 30 May 2005 UT and combined to characterize the comet before impact. On 04 Jul 2005 UT, a series of shorter exposures were taken to capture

short timescale changes in the spectrum after impact. Exposure times increase with airmass and range from 10 – 30 min during the first 3 hrs after impact. Here we use data from the KOA to focus on the 4050 Å band of C<sub>3</sub> (from 4049 – 4057 Å), which falls onto the central 1/8 of an echelle order, near the peak of aperture blaze.

Standard IDL procedures are used to bias correct and flat field each target and calibration exposure. Cosmic rays are removed using a two-step process. First, large cosmic ray hits are removed by considering the 13 target exposures together at each pixel and replacing large deviations from the mean with the median value. Then, to identify smaller cosmic ray hits, a 6×6 pixel spatial filter is used on each image, where pixels exceeding the mean value within the box by 2.5σ are replaced by the mean value. The echelle order is linear along the CCD over the narrow wavelength range considered here and it is sufficient to rectify the spectra by rotating the image 1.15°. Rectification is verified to be better than a pixel by comparing the dust continuum spatial profiles along the order. Flux calibration is performed for both the pre-impact and post-impact exposures using exposures of the flux standards, Feige 67 and BD+284211, respectively (Oke 1990). The total counts are integrated along the slit for the calibration standard and averaged over the bandpass of the Oke (1990) observations (4020-4060 Å). The HIRES observations confirm that there are no significant spectral features in either of the calibrations stars for this bandpass, so the mean observed count rates and the literature values for the total flux at 4050 Å are used to convert from observed count rate (DN/s) to flux density ( $\text{ergs s}^{-1} \text{ cm}^{-2} \text{ Hz}^{-1}$ ). We correct for the different airmass during the target and calibration exposures using a characteristic atmospheric extinction,  $k = 0.56$ , at 4000 Å.

The solar continuum dominates the cometary spectrum at most of the sampled wavelengths. We use the median value along the dispersion axis to calculate the spatial profile of reflected sunlight. The median profile is convolved with a high-resolution,  $R \sim 85,000$ , UVES

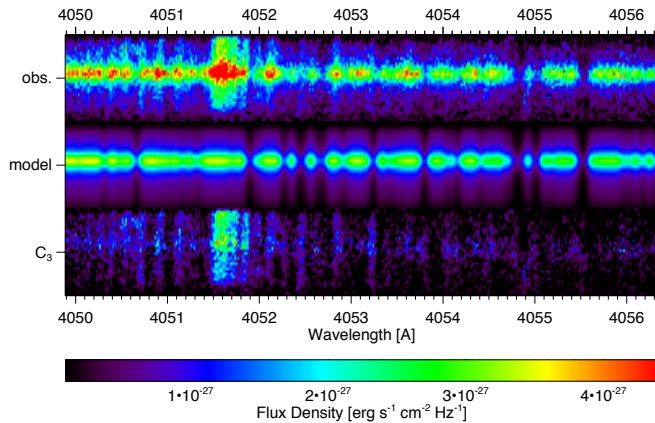


FIG. 1.— An example of the 2-dimensional solar continuum subtraction using the 30 May 2005 UT spectrum of comet 9P/Tempel 1 (obs.). The y-axis is the spatial dimension along the 7" spectrometer slit. The modeled solar spectrum (see text) is in the middle (model) and the continuum-subtracted 2-d emission spectrum of  $C_3$  plotted at the bottom ( $C_3$ ).

solar spectrum<sup>2</sup> and interpolated onto the HIRES plate scale to model the reflected sunlight. This model is subtracted from the observations, leaving only the gas emission. The higher signal-to-noise spectra taken on 30 May 2005 UT are used to demonstrate the dust continuum removal, Figure 1. Before removing the solar spectrum, some transitions in the emission spectrum of  $C_3$  (e.g., near 4052.5 and 4053.2 Å) are not apparent in the observations because they are collocated with solar features. After removing the solar spectrum these lines stand out against the background.

### 3. TEMPERATURES AND PRODUCTION RATES

The  $C_3$  excitation profile — that is, the distribution of population among rotational levels — can depend on the temperature and density in the coma, the heliocentric velocity and distance, and the formation mechanism of the molecule (e.g., the parent and grandparent molecules of  $C_3$ ). Rousselot et al. (2001) describe a complicated model that can be used to interpret the rotationally-resolved emission spectrum of cometary  $C_3$  by taking into account the heliocentric velocity and distance. However, those values do not change significantly over the timescale of these observations so they do not account for variation in the emission spectrum. We assume a simple thermal distribution in the excited state to model the emission spectrum, and allow for a variable excitation temperature to describes changes in the emission spectrum over the time period directly after *DI*.

Spectra of  $C_3$  are calculated using the line list of Tanabashi et al. (2005) for the  $A^1\Pi_u \leftarrow X^1\Sigma_g^+$  (000-000) transitions. The fraction of the total molecules that are in a particular  $J$  level is given by

$$F_J(T_r) = \frac{2J+1}{q_r} \exp\left(\frac{-hcB_0}{kT_r} J(J+1)\right) \quad (1)$$

where  $q_r$  is the rotational partition function given by

$$q_r = \sum_{J \text{ even}}^{\infty} (2J+1) e^{-hcB_0 J(J+1)/kT_r}$$

<sup>2</sup> [http://www.eso.org/observing/dfo/quality/UVES/pipeline/solar\\_spectrum\\_relation](http://www.eso.org/observing/dfo/quality/UVES/pipeline/solar_spectrum_relation)

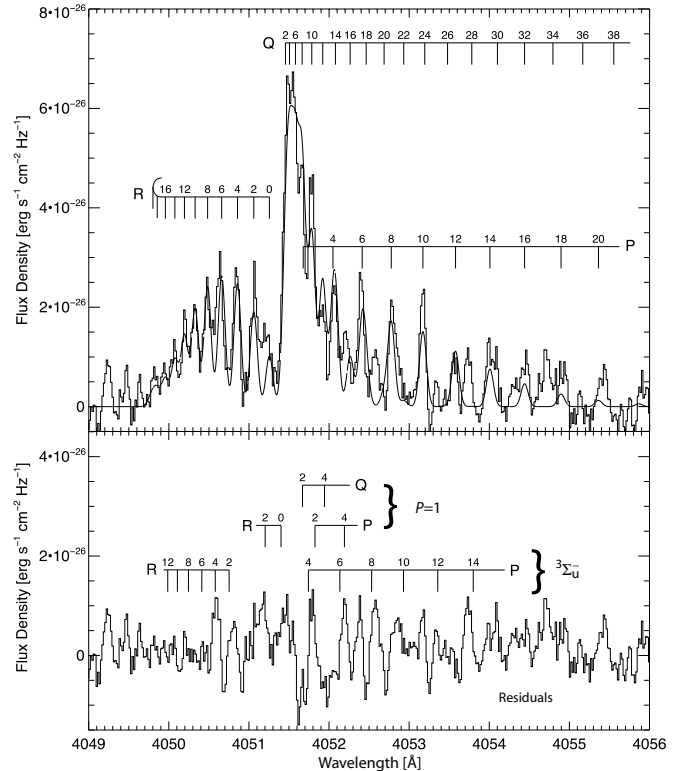


FIG. 2.— The spectrum of  $C_3$  before *DI* (on 30 May 2005 UT) integrated along the slit, with a best fit thermal excitation ( $T_r = 60 \pm 3$  K) model for the rotational population distribution (top). The observed spectrum is the average of three 20 min exposures. Residuals between the observations and the model, along with laboratory assignments of the transitions from two long-live perturbing states (bottom).

For  $C_3$  the ground state rotational constant  $B_0=0.43057$   $\text{cm}^{-1}$  (Schmuttenmaer et al. 1990).

Each modeled spectrum (e.g., Figure 2) has three free parameters; the excitation temperature,  $T_r$ , line width,  $w$ , and an intensity scaling factor,  $\alpha$ , which are used to reproduce the observed spectra. Spectra are calculated for a range of  $T_r$ ,  $w$ , and  $\alpha$  and compared to observations. The quality of fit is determined by  $\chi^2 = \sum_i (\delta y_i^2 / \sigma^2)$ , where  $\delta y_i$  is the residual at each sampled wavelength,  $i$ ,  $\sigma$  is approximated by the noise in the observed spectrum, and the best fit corresponds to  $\chi_{min}^2$ . Locations in parameter space where  $\chi^2 - \chi_{min}^2 = 1$  give the uncertainties in the input parameters.

The residuals from the fit indicate that the thermal population distribution is moderately successful at reproducing the observations and that there may be additional features in the spectrum, perhaps corresponding to transitions from perturbing states (Zhang et al. 2005).

We integrate the flux from  $C_3$  over 4049 – 4058 Å and use the standard fluorescence efficiency factor of  $g(r_H) = 1.0 \times 10^{-12} \times r_H^{-2}$   $\text{erg s}^{-1} \text{mol}^{-1}$  at a heliocentric distance,  $r_H = 1.55$  AU (A'Hearn et al. 1995), to find the total number of  $C_3$  molecules in the sampled area. A Haser model (Haser 1957) is used to determine the production rate of  $C_3$ . As detailed in Newburn & Spinrad (1984) the relationship between the production rate,  $Q$  ( $\text{s}^{-1}$ )

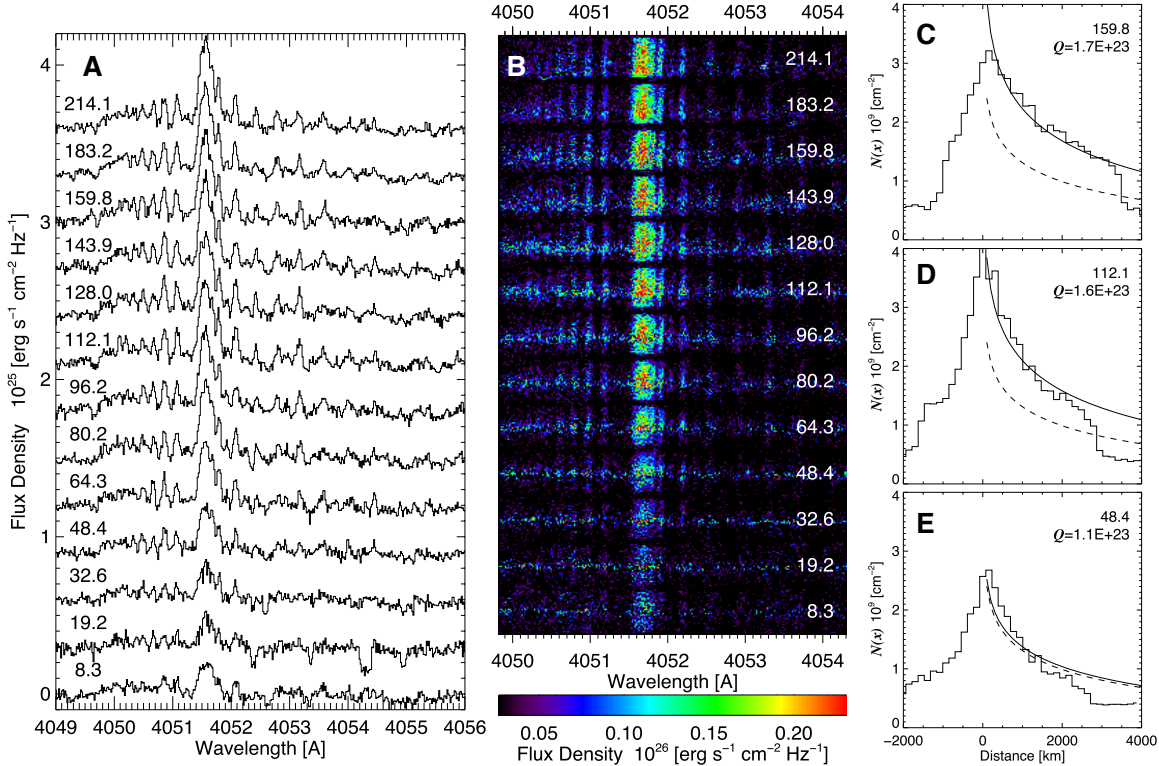


FIG. 3.— (A) Time series of spectra extracted along the slit. Spectra are labeled by the time at mid-exposure from *DI* in minutes. (B) the 2-dimensional spectra of C<sub>3</sub> after modeling and subtracting the contribution of reflected sunlight off of dust. (C)-(E) Examples of the column density of C<sub>3</sub>,  $N(x)$ , as a function of the distance from the nucleus, *datapoints*. For reference, a column density profile calculated using the pre-impact production rate of C<sub>3</sub> ( $1 \times 10^{23}$  mol/s) is plotted with a *dashed line* in each panel. The best fit profile calculated using a Haser model with a variable  $Q(C_3)$  is plotted with a *solid curve*.

and the column density profile,  $N(x)$  ( $\text{cm}^{-2}$ ), is given by

$$N(x) = \frac{Q}{4\pi\nu} \frac{2}{x} \left( \frac{l_r}{l_p - l_r} \right) \times \left[ \int_0^{x/l_r} K_0(y) dy - \int_0^{x/l_p} K_0(y) dy \right]$$

where  $x$  is the distance from nucleus (cm),  $l_p$  and  $l_r$  are the parent and radical scale lengths (cm), respectively, and  $K_0$  is the zero-order modified Bessel function of the second kind. The projected area that we observe is small, so these observations are not useful for constraining scale lengths and we use the values of  $l_p = 6.7 \times 10^3$  km and  $l_r = 6.5 \times 10^4$  km at a  $r_H = 1.55$  AU (A'Hearn et al. 1995).

The spectra taken in 13 exposures over the first 4 hrs after impact (until the comet set) change in both excitation profile and total flux. The high- $J$  lines in the  $R$ -branch band-head (near 4050 Å) are more prominent in the exposures roughly 100 min after impact (Figure 3A). The spatial profiles along the slit also change shortly after impact (Figure 3B). Three examples of the radial dependence of the C<sub>3</sub> column density are shown in Figures 3C – 3E, along with the best fit production rates,  $Q$ , and corresponding model profiles. The C<sub>3</sub> production rates determined using this technique fall in the range of  $1.1 - 1.7 \times 10^{23} \text{ s}^{-1}$ , which are consistent with the pre-impact measurements of Lara et al. (2006), however they are an order of magnitude smaller than the imaging measurements of (Schleicher et al. 2006).

#### 4. DISCUSSION

Since the heliocentric velocity of Tempel 1 does not change significantly over the 4 hrs of the observations, the changes in the excitation spectrum due to the Swings effect (e.g., changes in the radiative excitation of C<sub>3</sub> caused

by a Doppler shift of absorption lines in the solar spectrum) are small and some other process must account for the change in  $T_r$  after impact, Figure 4. Variations in the gas density around the ejecta are one way to explain changes in the excitation profile. C<sub>3</sub> lacks a permanent dipole moment so radiative relaxation is not an efficient method for removing population from high- $J$  states. At high densities however, collisional de-excitation can thermalize the population distribution. Ádámkóvics et al. (2003) have shown that in the interstellar medium the C<sub>3</sub> excitation profile depends on density, such that  $T_r$  exceeds the kinetic temperature at densities below  $500 \text{ cm}^{-3}$ .

If the gas density in the coma directly after impact is large, then  $T_r$  is essentially indicative of the thermal temperature. In the case of C<sub>3</sub>,  $T_r \sim 45$  K right before impact and increases over the first 100 min after impact up to 60 K — the same temperature it was in May. This increase may be due to decreasing gas density and the lack of collisional de-excitation. However, there is then a puzzling decrease in  $T_r$  from 100 – 200 min after impact. If the gas density were monotonically decreasing, then  $T_r$  should increase and then plateau. A method to test the possibility of gas density variation is to use an analogous molecule, such as C<sub>2</sub>, to make an independent measurement of the gas density. The 5100 Å Swan bands of C<sub>2</sub> are also recorded in the publicly available Keck spectra, which together with models such as those of Gredel et al. (1989) and Rousselot et al. (2001) could be used to quantitatively compare the excitation profiles of both C<sub>2</sub> and C<sub>3</sub>. Such an analysis would also provide a con-

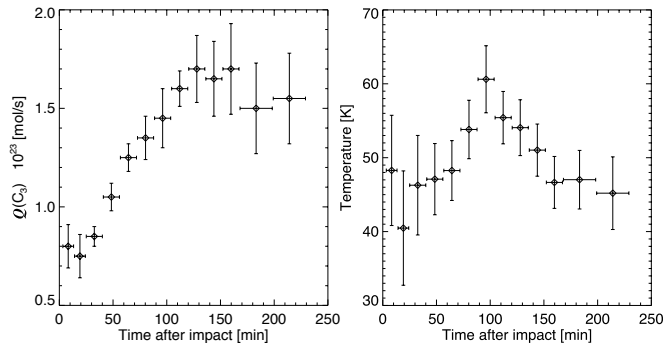


FIG. 4.— (Left) Comparison of the changes in  $C_3$  production rate and excitation temperature after impact.  $T_r$  is measured by fitting a thermal population distribution to the observed spectra and is plotted here as a function of the mid-exposure time after impact. See text for calculation of uncertainties. Error bars along the x-axis indicate the length of the exposure. (Right) The production rate,  $Q(C_3)$ , after  $DI$  determined by fitting the  $C_3$  column density profile,  $N(x)$ , with a Haser model (see Figure 3 for profiles).

straint on chemical models of carbon-bearing molecules in comets, since variations in the formation mechanism of  $C_3$  can change the excitation temperature. However, there is the possibility that the 15 K change in  $T_r$  occurs independently of the changes caused by  $DI$ . The quiescent  $T_r$  measured on 30 May 2005 is the same as the peak post-impact value of 60 K, so that perhaps  $T_r$  varies with time for  $C_3$ . The decrease in  $T_r$  at times greater than 100 min after impact supports the possibility that  $T_r$  is gradually fluctuating on the timescale of hours due to some stochastic variations.

The production rate for  $C_3$  reaches a plateau 130 min after  $DI$  and then declines after  $\sim 183$  min. The relative flux of CN follows a similar progression with time (Jehin et al. 2006), however CN reaches maximum production at a mid-exposure time of 96 min, significantly earlier than  $C_3$ . One simplistic interpretation is that there are more intermediate reactions between the photodissociation of the parent molecule and the formation of the

$C_3$ . The primary production pathway of cometary  $C_3$  is the photodissociation of either propyne ( $H_3CCCH$ ) or allene ( $H_2CCCH_2$ ) — in either case, one of the isomers of  $C_3H_4$  leads to the formation of  $C_3$  via the  $C_3H_2$  radical intermediate (Helbert et al. 2005). This common radical means that multiple pathways can produce the same rotational excitation spectrum of  $C_3$  (Song et al. 1994) and so the parent molecule of  $C_3$  cannot be distinguished. However, other mechanisms have been hypothesized for the formation of  $C_3$ , which could produce  $C_3$  with a different excitation spectrum. Helbert et al. (2005) mention the electron impact dissociation of  $C_3H_4$  as a source of  $C_3$  but note that rates for individual reactions have not been determined as so the relevance of this mechanism is uncertain. The propynal radical ( $C_3H_2O$ ) has also been proposed as a source of  $C_3$  (Krasnopolsky 1991), and proceeds via an excited state intermediate,  $C_3H_2^*$ . This radical could be the parent molecule of  $C_3$  with a different  $T_r$  than when produced from  $C_3H_2$ . In general, the total yield of  $C_3$  from  $C_3H_2O$  is only  $\sim 0.01$ .

It is unclear if there is link between the fact that  $Q(C_3)$  stops increasing 2 hrs after impact, roughly the same time that  $T_r$  starts to decrease, however these two profiles together provide a constraint on the chemistry of carbon-bearing molecules during  $DI$ . The excitation profile of  $C_3$  thus serves as a unique diagnostic of the chemistry and physical processes on short length-scales, and will test models of the chemistry in comets.

The data presented in this paper were obtained at the W. M. Keck Observatory, which was made possible by the financial support of the W. M. Keck Foundation. The authors wish to recognize and acknowledge the very significant cultural role and reverence that the summit of Mauna Kea has always had with the indigenous Hawaiian community.

#### REFERENCES

- Ádámkovics, M., Blake, G. A., & McCall, B. J. 2003, *ApJ*, 595, 235
- A’Hearn, M. F., Millis, R. L., Schleicher, D. G., Osip, D. J., & Birch, P. V. 1995, *Icarus*, 118, 223
- Cochran, A. L., Jackson, W. M., Meech, K. J., & Glaz, M., 2006, *Icarus*, (in press).
- Feldman, P. D., Lupu, R. E., McCandliss, S. R., Weaver, H. A., A’Hearn, M. F., Belton, M. J. S., & Meech, K. J. 2006, *ApJLett.*, 647, L61
- Gausset, L., Herzberg, G., Lagerqvist, A., & Rosen, B. 1965, *ApJ*, 142, 45
- Gredel, R., van Dishoeck, E. F., & Black, J. H. 1989, *ApJ*, 338, 1047
- Haser, L. 1957, *Bulletin de la Societe Royale des Sciences de Liege*, 43, 740
- Helbert, J., Rauer, H., Boice, D. C., & Huebner, W. F. 2005, *A&A*, 442, 1107
- Jehin, E., Manfroid, J., Hutsemékers, D., Cochran, A. L., Arpigny, C., Jackson, W. M., Rauer, H., Schulz, R., & Zucconi, J.-M. 2006, *ApJ*, 641, L145
- Krasnopolsky, V. A. 1991, *A&A*, 245, 310
- Lara, L. M., Boehnhardt, H., Gredel, R., Gutiérrez, P. J., Ortiz, J. L., Rodrigo, R., & Vidal-Nuñez, M. J. 2006, *A&A*, 445, 1151
- Mumma, M. J., DiSanti, M. A., Magee-Sauer, K., Bonev, B. P., Villanueva, G. L., Kawakita, H., Dello Russo, N., Gibb, E. L., Blake, G. A., Lyke, J. E., Campbell, R. D., Aycock, J., Conrad, A., & Hill, G. M. 2005, *Science*, 310, 270
- Newburn, R. L. & Spinrad, H. 1984, *AJ*, 89, 289
- Oke, J. B. 1990, *AJ*, 99, 1621
- Rousselot, P., Arpigny, C., Rauer, H., Cochran, A. L., Gredel, R., Cochran, W. D., Manfroid, J., & Fitzsimmons, A. 2001, *A&A*, 368, 689
- Schleicher, D. G., Barnes, K. L., & Baugh, N. F. 2006, *AJ*, 131, 1130
- Schmuttenmaer, C. A., Cohen, R. C., Pugliano, N., Heath, J. R., Cooksy, A. L., Busarow, K. L., & Saykally, R. J. 1990, *Science*, 249, 897
- Song, X., Bao, Y., Urdahl, R. S., Gosine, J. N., & Jackson, W. M. 1994, *Chem. Phys. Lett.*, 217
- Tanabashi, A., Hirao, T., Amano, T., & Bernath, P. F. 2005, *ApJ*, 624, 1116
- Vogt et al. 1994, *Proc. Soc. Photo-Opt. Instr. Eng.*, 2198, 362
- Zhang, G. Q., Chen, K. S., Merer, A. J., Hsu, Y. C., Chen, W. J., Shaji, S., & Liao, Y. A. 2005, *J. Chem. Phys.*, 122, 244308